ARTICLE

OBC
www.rsc.org/obc

Chiral clusters in a supersonic beam: R2PI-TOF spectroscopy of diastereomeric carboxylic esters/(*R*)-(+)-1-phenyl-1-propanol complexes

A. Giardini Guidoni,[a,b] A. Paladini,[a] F. Rondino,[a] S. Piccirillo,*[c] M. Satta[d] and M. Speranza*[e]

[a] *Dipartimento di Chimica, Università di Roma "La Sapienza", Pl. A. Moro 5, I-00185, Roma, Italy*

[b] *CNR-IMIP (Sezione Istituto Materiali Speciali), I-85050, Tito Scalo (Pz), Italy*

[c] *Università di Roma "Tor Vergata", Dipartimento di Scienze e Tecnologie Chimiche, Via della Ricerca Scientifica, I-00133, Rome, Italy. E-mail: piccirillo@fisica.uniroma2.it; Tel: +39-06-72594400*

[d] *CNR-ISC (Istituto dei Sistemi Complessi), I-00185, Roma, Italy*

[e] *Facoltà di Farmacia, Dipartimento di Studi di Chimica e Tecnologia delle Sostanze Biologicamente Attive, Università di Roma "La Sapienza", pl. A. Moro 5, I-00185, Roma, Italy. E-mail: maurizio.speranza@uniroma1.it; Fax: +39-06-49913602; Tel: +39-06-49913497*

Received 3rd August 2005, Accepted 30th August 2005
First published as an Advance Article on the web 3rd October 2005

Wavelength and mass resolved resonance-enhanced two photon ionization (R2PI) excitation spectra of (*R*)-(+)-1-phenyl-1-propanol ($\mathbf{P}_R$) and its complexes with some chiral esters, *i.e.* methyl lactates ($\mathbf{L}_R$ and $\mathbf{L}_S$), methyl 3-hydroxybutyrates ($\mathbf{H}_R$ and $\mathbf{H}_S$), and methyl 2-chloropropionates ($\mathbf{C}_R$ and $\mathbf{C}_S$), have been recorded after a supersonic molecular beam expansion and interpreted in the light of DFT calculations. The spectral features of the selected complexes were found to depend on the nature of hydrogen-bond interactions within the diasteromeric complexes, whose intensity in turn depends upon the structure and the configuration of the estereal moiety. The study further confirms resonant two-photon ionization spectroscopy, coupled with time-of-flight mass resolution (R2PI-TOF), as an excellent tool for gathering valuable information on the interactive forces in molecular clusters and for the enantiodiscrimination of chiral molecules in the gas phase.

Introduction

Carboxylic compounds substituted at the α-position play a prominent role in a variety of important medical and pharmaceutical applications.[1–6] From the point of view of basic research, these compounds look very attractive and challenging owing to the α-substituent adjacent to the carboxylic group which allows many possible intramolecular interactions in the isolated molecule and a variety of intermolecular interactions in its clusters with suitable acceptors. Simple α-substituted carboxylic acids have been extensively studied, both theoretically and experimentally.[7–12] Similar efforts have not been made on the study of their methyl esters.[13] This has happened despite the fact that substitution of the COOH group by $COOCH_3$ prevents some intramolecular hydrogen bonding and, therefore, makes the detailed study of their intermolecular interactions in isolated clusters much easier.

The practical importance of α-substituted carboxylic compounds in medical and pharmaceutical sciences is increased by the fact that most of these molecules are chiral and that many biochemical processes are based on the enantioselective recognition of asymmetric molecules by chiral receptors. Therefore, the study of the fundamental mechanism of enantioselectivity in noncovalent diastereomeric complexes, and of the underlying intermolecular interactions, are crucial for a better understanding of the recognition phenomena in life sciences as well as their potential impact on the development of novel procedures for racemate analyses and for enantioselective syntheses. This aim can be achieved through the application of some gas-phase methodologies, including mass spectrometry,[14–20] which provides information about the stability and reactivity of diastereomeric cluster ions, and supersonic expansion laser spectroscopy,[14,21–24] which gives information on their neutral counterparts.

The latter methodology relies on the spectral signature of noncovalent diastereomeric complexes formed by supersonic co-expansion of a chiral chromophore and a chiral "solvent" molecule (*solv*). The homo- and heterochiral pairs are characterized by the non-equivalence of their structure and, therefore, involve different intermolecular interactions both in the ground and excited states. As a consequence, they exhibit different shifts of the $S_1 \leftarrow S_0$ transition relative to that of the bare chromophore, which allow their assignment and optical selection.[25] The use of supersonic expansion in these studies is essential, since it leads to the formation of isolated molecular complexes in their electronic ground state at the lowest rotational and vibrational levels. As a result, their excitation spectra often display only few, well resolved narrow bands. Furthermore, the low internal temperature of the adducts, ranging around a few Kelvin,[26,27] favours population of the enthalpically most stable structural isomer and sometimes stabilization of other structural variants, if their interconversion requires the overcoming of sizable energy barriers.

The spectroscopic techniques used to date include laser-induced fluorescence (LIF)[22,25,28,29] and resonant two-photon ionization (R2PI),[30–32] this latter allowing the measurements of the binding energy of the supersonically expanded adducts. Structural aspects have been elucidated by vibrational spectroscopy, either FTIR[33,34] or IR/UV double resonance experiments,[35–37] or alternatively microwave experiments.[38] In recent years, the R2PI spectroscopy, coupled with time-of-flight (TOF) mass spectrometric detection, has been extensively employed to investigate the role of multiple intermolecular interactions in chiral recognition of bifunctional *solv* molecules by a suitable chromophore, *i.e.* (*R*)-(+)-1-phenyl-1-propanol ($\mathbf{P}_R$). The compounds investigated so far were diols[39–42] and 3-hydroxytetrahydrofuran.[43] These bifunctional molecules may

DOI:10.1039/b511050e

present intramolecular hydrogen bonding in the isolated state and may exist in distinct conformations.

When associated with $\mathbf{P}_R$, their intramolecular hydrogen bond tends to be disrupted for the benefit of the intermolecular interactions with the chromophore. According to the relevant hydrogen bond network, these complexes can be classified into three groups:[35–37] (i) those where the chromophore acts as the H-donor to the most basic site of *solv* (:Y in Fig. 1). These structures exhibit also a weak O–H $\cdots\pi$ interaction between the alcoholic group of *solv* and the π system of the chromophore (Y^{add} in Fig. 1); (ii) those where the chromophore acts as the H-donor to the less basic n-type site of *solv* (O in Fig. 1). These structures show an intramolecular O–H $\cdots$ Y interaction between the functional groups of *solv* (O^{add} in Fig. 1); and (iii) the complexes in which the OH group of the chromophore acts either as the H-donor to the most basic site of *solv* and as the H-bond acceptor from its OH alcoholic function (O^{ins} in Fig. 1). With *solv* = 3-hydroxytetrahydrofuran, all three structures are generated. Relative to the $S_1 \leftarrow S_0$ electronic band origin of the most stable *anti* conformer of the bare $\mathbf{P}_R$ chromophore, the Y^{add}-like structure displays a pronounced hypsochromic shift due primarily to the intermolecular O–H $\cdots\pi$ bonding, the O^{add}-like one an appreciable bathochromic shift, and the O^{ins}-like one a relatively limited band shift due to the dual H-bond donor/acceptor character of the chromophore. In all instances, the largest shifts are observed with the heterochiral structures. With symmetrical diols, *e.g.* 2,3-butanediols and 2,4-pentanediols, class (i) and (ii) structures coincide (:Y=OH). In this case, the spectral features of the relevant complexes with $\mathbf{P}_R$ were found to depend on cooperative O–H $\cdots$ O–H $\cdots$ O–H $\cdots\pi$ interactions between the two components, the intensity of which depends upon the specific configuration of the diol moiety and the relative position of its hydroxyl groups (2,3-butanediols < 2,4-pentanediols). The result is that 2,3-butanediols, in which the O–H $\cdots\pi$ interaction is relatively weak for structural reasons, display red shifts, whereas 2,4-pentanediols exhibit distinct blue shifts, since here optimal O–H $\cdots\pi$ arrangement is not hindered by the cooperative O–H $\cdots$ O–H $\cdots$ O–H interactions.

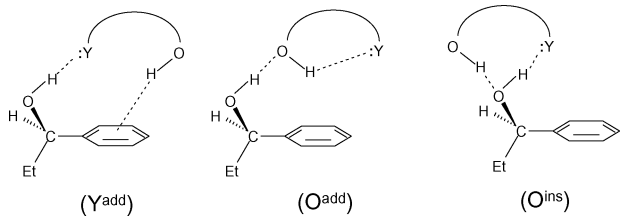

Fig. 1 Schematic representation of the most common structures for gas-phase complexes between (*R*)-(+)-1-phenyl-1-propanol ($\mathbf{P}_R$) and bifunctional alcohols (:Y most basic center of the alcoholic *solv*).

In view of the importance of α-substituted carboxylic compounds in life sciences, we decided to extend the R2PI-TOF investigation to these compounds and specifically to their methyl esters. In particular, we selected as model esters the methyl lactates ($\mathbf{L}_R$ and $\mathbf{L}_S$; Fig. 2) which, relative to diols and 3-hydroxytetrahydrofuran, involve other types of intramolecular hydrogen bonds, such as O–H $\cdots$ O=C. Their behavior is contrasted with that of methyl 3-hydroxybutyrates ($\mathbf{H}_R$ and $\mathbf{H}_S$; Fig. 2) and of methyl 2-chloropropionates ($\mathbf{C}_R$ and $\mathbf{C}_S$; Fig. 2). The former were chosen as representative β-hydroxy substituted carboxylic esters and the latters as representative α-substituted carboxylic esters lacking of intramolecular hydrogen bondings.

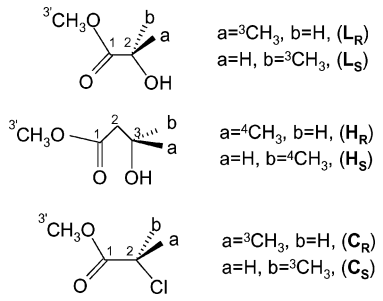

Fig. 2 The selected *solv* molecules.

Experimental

R2PI-TOF experiments

The experimental set up to produce the molecular clusters and to perform their spectral analysis has been described elsewhere.[44] The supersonic beam of the species of interest was obtained by adiabatic expansion of a carrier gas (Ar; stagnation pressure from 2 to 4 bar), seeded with $\mathbf{P}_R$ and one enantiomer of the selected carboxylic esters through a pulsed nozzle (i.d. 400 μm; aperture time: 200 μs; repetition rate: 10 Hz) heated at T = 120 °C. Their concentration is maintained low enough to minimise the production of heavier clusters. The molecular beam was allowed to pass through a 1-mm diameter skimmer into a second chamber equipped with a vertical TOF spectrometer. Molecules and clusters in the beam are excited and ionised by one or two tuneable dye lasers, pumped by a Nd-YAG laser (λ = 532 nm). The dye fundamental frequencies are doubled and, when necessary, mixed with residual 1064 nm radiation to obtain two different frequencies ν_1 and ν_2. The ions formed by R2PI ionizations are mass discriminated and detected by a channeltron after a 50-cm flight path. The mass selected ionic signals are recorded and averaged by a digital oscilloscope and stored on a PC

One colour R2PI experiments (1cR2PI) involve electronic excitation of the species of interest by absorption of one photon $h\nu_1$ and by its ionisation by a second photon of the same energy $h\nu_1$. The 1cR2PI excitation spectra were obtained by recording the entire TOF mass spectrum as a function of ν_1. The wavelength dependence of a given mass resolved ion represents the absorption spectrum of the species and contains important information about its electronic excited state S_1.

Computational details

MM3 force-field classical molecular dynamics is run for each neutral adduct at a temperature of 800 K with some constraints to overcome dissociation; the cumulative time is 0.1 ns with a time step of 0.5 fs and a dump time of 1 ps. The 100 snapshots are then optimized with a convergence of 10^{-6} kcal mol^{-1} Å^{-1} RMS gradient per atom. The obtained optimized structures are classified according to their energy and conformation. Each molecular and cluster conformer is optimized with a density functional theory (DFT) approach using a medium size basis set. The DFT Hamiltonian is Becke's three-parameter hybrid functional with the Lee, Yang, and Parr correlation functional (B3LYP); the basis set is the 6–31G. All the ab initio calculations were performed using the GAUSSIAN 98 package.[45]

Results and discussion

Fig. 3a illustrates the excitation spectrum of the bare $\mathbf{P}_R$, taken around the electronic $S_1 \leftarrow S_0$ origin. The band origin region of the spectrum displays a peak at 37577 cm^{-1} (A) and two other major peaks at 37618 cm^{-1} (B) and at 37624 cm^{-1} (C). This triplet of bands has been assigned to the 0_0^0 electronic $S_1 \leftarrow S_0$ origin of three most stable conformers of the chromophore, obtained by rotation around its C_α–C_β bond placed quasi-perpendicular to the aromatic ring.[30] In particular, the most intense band (B) is associated with the most stable *anti* rotamer, whereas the less intense bands (A) and (C) to the two *gauche* conformers.

The 1cR2PI excitation spectra of the isomeric complexes of $\mathbf{P}_R$ with the selected carboxylic esters are illustrated in Fig. 3–5. Their spectral patterns are characterized by an ensemble of

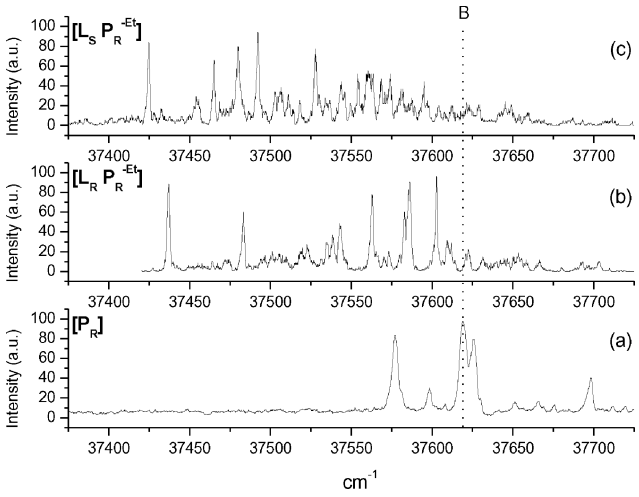

Fig. 3 1cR2PI excitation spectra of bare $\mathbf{P}_R$ (a) and its complexes with $\mathbf{L}_R$ (b) and $\mathbf{L}_S$ (c). The origin of the frequency scale is relative to the peak B at 37618 cm^{-1} of bare $\mathbf{P}_R$ which is marked as a dashed line.

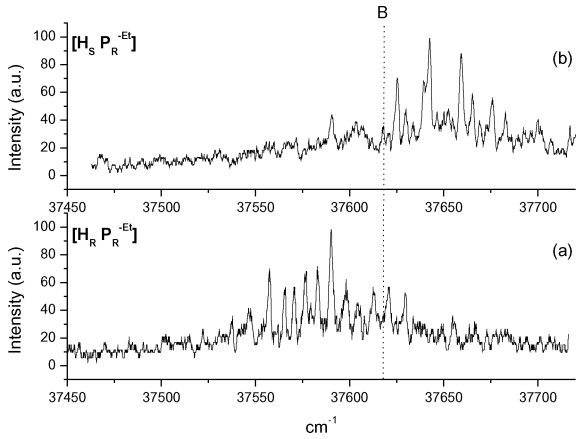

Fig. 4 1cR2PI excitation spectra of the complexes between $\mathbf{P}_R$ and $\mathbf{H}_R$ (a) and $\mathbf{H}_S$ (b). The origin of the frequency scale is relative to the peak B at 37618 cm^{-1} of bare $\mathbf{P}_R$ which is marked as a dashed line.

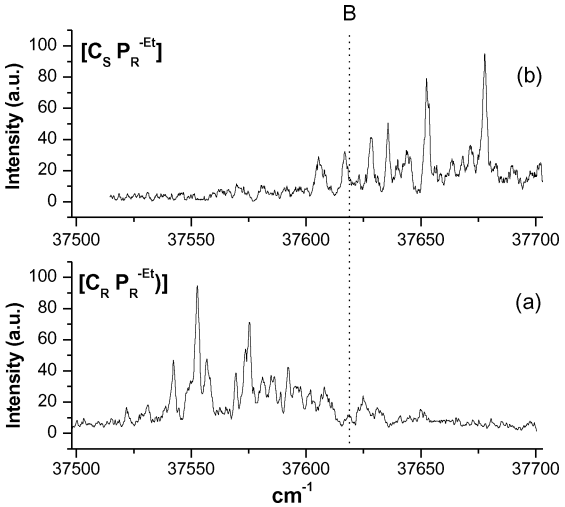

Fig. 5 1cR2PI excitation spectra of the complexes between $\mathbf{P}_R$ and $\mathbf{C}_R$ (a) and $\mathbf{C}_S$ (b). The origin of the frequency scale is relative to the peak B at 37618 cm^{-1} of bare $\mathbf{P}_R$ which is marked as a dashed line.

bands red- or blue-shifted relative to the 0_0^0 electronic $S_1 \leftarrow S_0$ origin of the most populated *anti* conformer of the bare chromophore $\mathbf{P}_R$ (peak B at 37618 cm^{-1}).[30] A red shift (negative $\Delta\nu$) is due to an increase of the complex bonding in going from the S_0 ground state to the S_1 excited state. A blue shift (positive $\Delta\nu$) is due to a decrease of the complex bonding by the same excitation process. The magnitude of the $\Delta\nu$ values is somewhat related to the variation of bonding efficiency in the π and π^* states.

As pointed out in related papers,[30,39] the bathochromic shifts of the 0_0^0 electronic $S_1 \leftarrow S_0$ origin, observed when $\mathbf{P}_R$ is associated with an alcoholic *solv*, is phenomenologically related to the increase of the electron density on the oxygen center of the chromophore (henceforth denoted as **O**) by **O**–H $\cdots$ O hydrogen bonding with the O atom of the solvent. Similarly important are dispersive interactions between the aliphatic chain of the solvent and the π-system of the chromophore, which are mainly responsible of the different spectral shifts observed in diastereomeric complexes involving chiral moieties.[30]

This general behavior is further corroborated by the 1cR2PI absorption spectra of the homochiral $[\mathbf{L}_R \cdot \mathbf{P}_R]$ and heterochiral $[\mathbf{L}_S \cdot \mathbf{P}_R]$ complexes (Fig. 3b–c, respectively), obtained by monitoring the ion signal at the ethyl loss fragment mass ($m/z = 211$). Similar spectra have been obtained by monitoring the parent ion signal at $m/z = 240$. Their spectral patterns are characterized by the presence of five intense bands all red-shifted relative to the band origin B of the bare chromophore $\mathbf{P}_R$. No blue-shifted signals were observed for these 1 : 1 complexes.

Concerning the nature of these five signals, it is well established that association of $\mathbf{P}_R$ with bidentate *solv*, like the selected esters, can markedly unbalance the relative population of the A–C rotamers of the chromophore to the point that only one $\mathbf{P}_R$ conformer predominates.[30,43] This view is further confirmed by DFT calculations of the most stable diastereomeric $[\mathbf{L}_R \cdot \mathbf{P}_R]$ and $[\mathbf{L}_S \cdot \mathbf{P}_R]$ isomers. Fig. 6 shows that the number of stable $[\mathbf{L}_R \cdot \mathbf{P}_R]$ and $[\mathbf{L}_S \cdot \mathbf{P}_R]$ isomers coincides with the number of intense signals of Fig. 3. Among the DFT computed structures, the (a) and (b) rotamers, like the (a′) and (b′) ones, are structurally analogous to the members of the O^{ins} family. Structures (c) and (c′) can be considered as belonging to the O^{add} class, whereas structures (d), (d′), (e), and (e′) may be included in the Y^{add} category. It is worth recalling that the Y^{add} structures may be characterized by an intense O–H $\cdots$ π interaction which normally promotes the blue-shifting (or reduces the red-shifting) of their band origin.[39–43] In this frame, we tend to assign the least red-shifted band of Fig. 3b to structures (e) and that of Fig. 3c to structure (e′), since both are characterized by the alcoholic OH bond pointing to the π-system of $\mathbf{P}_R$ at relatively short O–H $\cdots$ π equilibrium distances (Table 1).

At first glance, however, this assignment seem to contrast with the observation that, in spite of its short O–H $\cdots$ π distance (3.25 Å, Table 1), the heterochiral structure (e′) exhibits a red-shifts larger than those of the homochiral congener

Table 1 B3LYP/6-31G-calculated total energy values and geometric parameters of the most stable optimized structures of the diastereomeric $[\mathbf{L}_{R/S} \cdot \mathbf{P}_R]$ complexes. Symbols in the table are explained in the text

		a	*b*	*c*	*d*	*e*
OH $\cdots$ π	RR	4.48	4.33	4.43	6.91	4.16
	RS	4.48	4.25	3.47	2.83	3.25
C(3′) $\cdots$ π	RR	6.87	8.02	8.78	6.12	5.82
	RS	7.18	8.10	7.07	5.37	6.57
C=O $\cdots$ π	RR	4.70	6.02	6.20	6.87	4.53
	RS	4.76	5.90	4.63	4.33	4.63
$CH_3O \cdots \pi$	RR	6.62	7.29	7.88	5.08	5.30
	RS	6.85	7.26	6.49	4.49	5.83
C(2)H $\cdots$ π	RR	6.54	7.00	5.80	3.38	6.19
	RS	6.31	4.00	6.63	5.41	3.00
O–H–**O**	RR	1.83	1.86	—	—	1.86
	RS	1.82	1.89	—	—	2.57
O–H–O	RR	1.90	1.88	1.88	2.06	1.87
	RS	1.95	1.87	1.88	2.05	1.92
O–H–O	RR	2.71	2.65	2.04	2.08	2.57
	RS	2.60	2.70	2.06	2.72	2.73
C(3) $\cdots$ π	RR	6.90	7.07	6.15	4.27	5.94
	RS	6.75	4.91	6.46	5.19	3.97

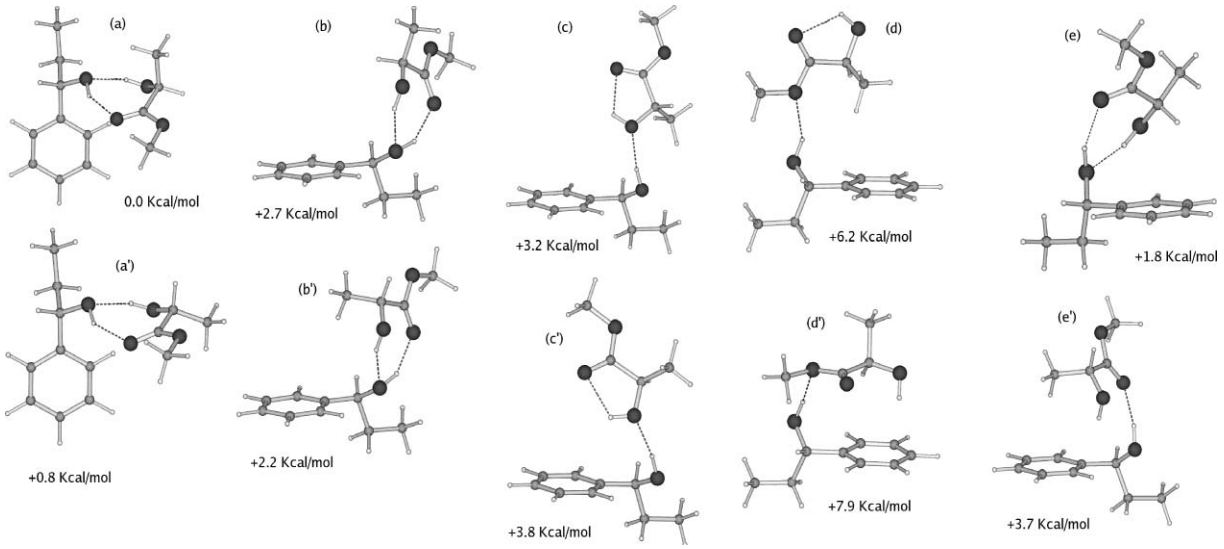

Fig. 6 B3LYP/6-31G-calculated structures of the diastereomeric $[\mathbf{L}_{R/S}\cdot\mathbf{P}_R]$ clusters: (a–e) $[\mathbf{L}_R\cdot\mathbf{P}_R]$; (a′–e′) $[\mathbf{L}_S\cdot\mathbf{P}_R]$.

(e) (O–H $\cdots\pi$ distance = 4.16 Å, Table 1). This apparent discrepancy may be readily removed by considering the effective dispersive interaction between the C(3)H_3 group of lactate and the π-system of $\mathbf{P}_R$ in the heterochiral form (e′) (C(3) $\cdots\pi$ distance = 3.97 Å, Table 1), which instead is virtually absent in the homochiral forms (e) (C(3) $\cdots\pi$ distance = 5.94 Å, Table 1).

The structural assignment of the residual red shifted bands of Fig. 3b–c is more complicated. However, in analogy with previous evidence, we tend to assign to the most red-shifted bands to the O^{add}-like structures (c) and (c′). This assignment is somewhat supported by the fact that, compared to $[\mathbf{L}_R\cdot\mathbf{P}_R]$, the heterochiral $[\mathbf{L}_S\cdot\mathbf{P}_R]$ complex displays the largest red shift ($\Delta\nu$ = − 193 cm^{-1}; Fig. 3c) much like the corresponding complexes with *solv* = 2-butanol.[30,31]

Figs. 4a–b report the 1cR2PI absorption spectra of the homochiral $[\mathbf{H}_R\cdot\mathbf{P}_R]$ and heterochiral $[\mathbf{H}_S\cdot\mathbf{P}_R]$ complexes, obtained by monitoring the ion signal at the ethyl loss fragment mass (*m*/*z* 225). Similar spectra have been obtained by monitoring the parent ion signal at *m*/*z* = 254. The spectral pattern of the heterochiral $[\mathbf{H}_S\cdot\mathbf{P}_R]$ complex is characterized by the presence of several bands most of them blue-shifted relative to the band origin B of the bare chromophore $\mathbf{P}_R$. Instead, the spectral pattern of the homochiral $[\mathbf{H}_R\cdot\mathbf{P}_R]$ complex presents several bands slightly red-shifted relative to the band origin B of the bare chromophore $\mathbf{P}_R$.

This opposite behaviour can be rationalized in terms of the corresponding O^{add} structures (Fig. 7). According to Table 2, relative to the heterochiral $[\mathbf{H}_S\cdot\mathbf{P}_R]$ structure, the homochiral $[\mathbf{H}_R\cdot\mathbf{P}_R]$ form shows a shorter C(2) $\cdots\pi$ distance (3.98 Å, Table 2) and a longer O–H $\cdots\pi$distance (5.10 Å, Table 2) which indicate that first interaction may effectively outbalance the latter in this complex. This is not any longer true in the heterochiral $[\mathbf{H}_S\cdot\mathbf{P}_R]$ structure (C(2) $\cdots\pi$ distance = 4.09 Å; O–H $\cdots\pi$distance = 4.53 Å, Table 2). The consequence is that the counterbalancing effects of dispersive and polar interactions induce a small red-shift in the band origin of $[\mathbf{H}_R\cdot\mathbf{P}_R]$, whereas the predominance of the polar interaction over the dispersive one induces small blue-shift in the band origin of $[\mathbf{H}_S\cdot\mathbf{P}_R]$.

Fig. 5a–b show the 1cR2PI absorption spectrum of $[\mathbf{C}_S\cdot\mathbf{P}_R]$ and $[\mathbf{C}_R\cdot\mathbf{P}_R]$, respectively, taken by monitoring the ion signal at the ethyl loss fragment mass (*m*/*z* = 229). Similar spectra have been obtained by monitoring the parent ion signal at *m*/*z* = 258. The spectral patterns of Fig. 5 show close similarities with those of the $[\mathbf{H}_S\cdot\mathbf{P}_R]$ and $[\mathbf{H}_R\cdot\mathbf{P}_R]$ pair reported in Fig. 4. Indeed, the heterochiral $[\mathbf{C}_S\cdot\mathbf{P}_R]$ complex is characterized by the presence of several bands most of them blue-shifted relative to the band origin B of the bare chromophore $\mathbf{P}_R$. Instead, the spectral pattern of the homochiral $[\mathbf{C}_R\cdot\mathbf{P}_R]$ complex presents several bands red-shifted relative to the band origin B of the bare chromophore $\mathbf{P}_R$. The geometrical structures and relative energies of the homochiral and heterochiral adducts are shown

Table 2 B3LYP/6-31G-calculated total energy values and geometric parameters of the most stable optimized structures of the diastereomeric $[\mathbf{H}_{R/S}\cdot\mathbf{P}_R]$ complexes. Symbols in the table are explained in the text

	Homo	*Hetero*
O–H–O	1.73	1.75
O–H–O	1.97	1.95
C=O $\cdots\pi$	5.79	4.47
$CH_3O\cdots\pi$	5.78	4.46
C(3) $\cdots\pi$	4.25	4.91
C(2) $\cdots\pi$	3.98	4.09
OH $\cdots\pi$	5.10	4.53
C(4) $\cdots\pi$	5.69	5.42
C(3′) $\cdots\pi$	7.07	5.08

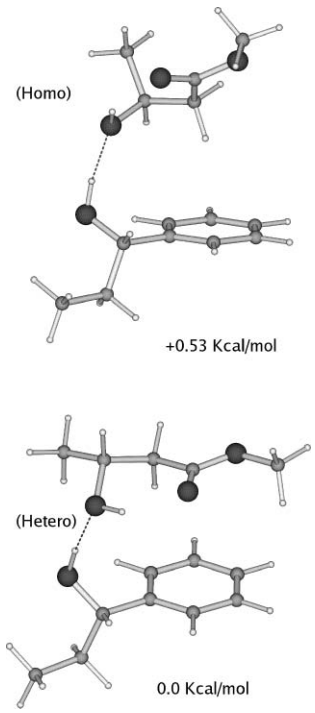

Fig. 7 B3LYP/6-31G-calculated most stable structures of the diastereomeric $[\mathbf{H}_{R/S}\cdot\mathbf{P}_R]$ clusters: (a) $[\mathbf{H}_R\cdot\mathbf{P}_R]$; (a′) $[\mathbf{H}_S\cdot\mathbf{P}_R]$.

in Fig. 8. In particular, the three most stable homochiral [$\mathbf{C_R}\cdot\mathbf{P_R}$] structures are shown in Fig. 8a, 8b and 8c and those concerning the heterochiral [$\mathbf{C_S}\cdot\mathbf{P_R}$] ones are illustrated in Fig. 8a′, 8b′ and 8c′. Their conformational topology is very similar: in the most stable structures (Fig. 8a and 8a′), the OH group of $\mathbf{P_R}$ is H-bonded to the carbonyl oxygen of $\mathbf{C_{R/S}}$, while their CH_3O group is outside the π-region of the chromophore. The immediately less stable structures (Fig. 8b and 8b′) are hydrogen-bonded much like their most stable isomers, but their CH_3O group are placed over the chromophore aromatic ring. The highest energy adducts show hydrogen bonding between the OH of $\mathbf{P_R}$ and the CH_3O oxygen of $\mathbf{C_{R/S}}$ (Fig. 8c and 8c′). A conceivable explanation of the experimental spectral shifts of Fig. 5 can be given in terms of the structural parameters of the diastereomeric clusters (Table 3). The red shifts in the π–π* transition of the homochiral [$\mathbf{C_R}\cdot\mathbf{P_R}$] cluster with respect to the bare $\mathbf{P_R}$ could be accounted for by the dispersive interactions between the aromatic ring and the methyl group at C(3) of $\mathbf{C_R}$ (C(3)$\cdots\pi$ distance (in Å) = 4.15 (a), 4.69 (b); Table 3).[30,46–48] No similar red-shifts are observed with the heterochiral [$\mathbf{C_S}\cdot\mathbf{P_R}$] cluster in conformity with the much weaker interactions between the aromatic ring of $\mathbf{P_R}$ and the more removed methyl group at C(3) of $\mathbf{C_S}$ (C(3)$\cdots\pi$ distance (in Å) = 4.54 (a′), 4.91 (b′); Table 3). The fact that the more pronounced differences in the C(3)$\cdots\pi$ distance are exhibited by the (a) (*vs.* (a′)) and (b) (*vs.* (b′)) structures allows us to assign these structures to the most red-shifted bands of the homochiral [$\mathbf{C_R}\cdot\mathbf{P_R}$] cluster. Besides, the blue-shifted bands of the heterochiral [$\mathbf{C_S}\cdot\mathbf{P_R}$] cluster can be attributed to the polar interaction between the π-ring of the heterochiral [$\mathbf{C_S}\cdot\mathbf{P_R}$] structure (c′) and the rather acidic ClCH hydrogen pointing towards it (ClCH$\cdots\pi$ distance = 2.89 Å, Table 3). The same interaction is prevented in the homochiral congener (c) (ClCH$\cdots\pi$ distance = 6.45 Å, Table 3), which in fact does not display any blue-shifted band relative to the bare chromophore.

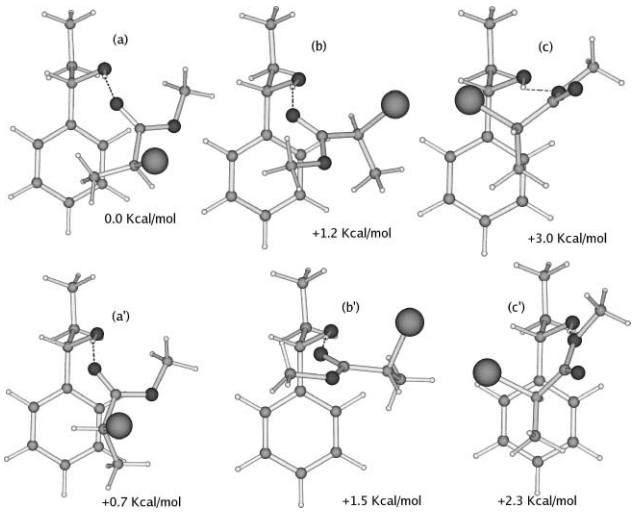

Fig. 8 B3LYP/6-31G-calculated structures of the diastereomeric [$\mathbf{C_{R/S}}\cdot\mathbf{P_R}$] clusters: (a–c) [$\mathbf{C_R}\cdot\mathbf{P_R}$]; (a′–c′) [$\mathbf{C_S}\cdot\mathbf{P_R}$].

Conclusions

The present study shows how the analysis of the mass resolved R2PI-TOF excitation spectra of the most stable, supersonically expanded complexes between (*R*)-(+)-1-phenyl-1-propanol and the enantiomers of methyl lactate, methyl 3-hydroxybutyrate, and methyl 2-chloropropionate, coupled with DFT calculations, can provide valuable information on their structures and the interactive forces holding them together. The study further supports the view that the spectral features of the selected complexes depend on a complicate interplay between polar and dispersive interactions within the diasteromeric complexes, whose intensity in turn depends on the structure and the configuration of the estereal moiety. On these grounds, mass resolved R2PI-TOF spectroscopy confirms itself as an excellent method for the enantiodiscrimination of chiral molecules in the gas phase.

Table 3 B3LYP/6-31G-calculated total energy values and geometric parameters of the most stable optimized structures of the diastereomeric [$\mathbf{C_{R/S}}\cdot\mathbf{P_R}$] complexes. Symbols in the table are explained in the text

	a	*b*	*c*	*a′*	*b′*	*c′*
O–H–O	1.87	1.88	1.97	1.86	1.88	1.90
C(3)$\cdots\pi$	4.15	4.69	4.55	4.54	4.91	4.55
Cl$\cdots\pi$	6.48	6.61	5.29	6.61	7.30	4.69
C=O$\cdots\pi$	4.27	4.51	7.15	4.26	4.65	6.05
$CH_3O\cdots\pi$	4.86	5.47	5.15	4.86	6.21	4.79
C(3′)$\cdots\pi$	5.35	6.06	6.07	5.30	6.48	6.09
ClCH$\cdots\pi$	4.65	4.31	6.45	4.56	6.31	2.89
OH–Cl	5.35	4.07	3.18	5.41	4.21	3.91

Acknowledgements

Contract grant sponsors: Ministero della Università e della Ricerca Scientifica e Tecnologica (MURST-COFIN) and Consiglio Nazionale delle Ricerche (CNR).

References

1 E. Scott, *J. Am. Acad. Dermatol.*, 1984, **11**, 867.
2 Y. Guzel, *J. Mol. Struct. (THEOCHEM)*, 1996, **366**, 131.
3 L. Moy, H. Murad and R. Moy, *J. Dermatol. Surg. Oncol.*, 1996, **19**, 243.
4 E. Scott, *Can. J. Dermatol.*, 1989, **43**, 222.
5 M. Kleerebezem and J. Hugenholtz, *Curr. Opin. Biotechnol.*, 2003, **14**, 232.
6 D. Gilding and M. Reed, *Polymer*, 1979, **20**, 1459.
7 A. Borba, A. Gómez-Zavaglia, L. Lapinski and R. Fausto, *Phys. Chem. Chem. Phys.*, 2004, **6**, 2101.
8 C. Blom and A. Bauder, *J. Am. Chem. Soc.*, 1982, **104**, 2993.
9 H. Hasegawa, O. Ohashi and I. Yamaguchi, *J. Mol. Struct.*, 1982, **82**, 205.
10 H. Hollenstein, T. Ha and H. S. Günthard, *J. Mol. Struct.*, 1986, **146**, 289.
11 H. Iijima, M. Kato and B. Beagley, *J. Mol. Struct.*, 1993, **295**, 289.
12 S. Jarmelo and R. Fausto, *Phys. Chem. Chem. Phys.*, 2000, **2**, 1155.
13 A. Borba, A. Gómez-Zavaglia, L. Lapinski and R. Fausto, *Vib. Spectrosc.*, 2004, **36**, 79.
14 M. Speranza, *Adv. Phys. Org. Chem.*, 2004, **39**, 147.
15 M. Speranza, *Int. J. Mass Spectrom.*, 2004, **232**, 277.
16 M. Sawada, *Mass Spectrom. Rev.*, 1997, **16**, 733.
17 C. A. Schalley, *Int. J. Mass Spectrom.*, 2000, **194**, 11.
18 A. Filippi, A. Giardini, S. Piccirillo and M. Speranza, *Int. J. Mass Spectrom.*, 2000, **198**, 137.
19 C. B. Lebrilla, *Acc. Chem. Res.*, 2001, **34**, 653.
20 D. Dearden, Y. Liang, J. B. Nicoll and K. A. Kellersberger, *J. Mass Spectrom.*, 2001, **36**, 989.
21 M. Speranza, M. Satta, S. Piccirillo, F. Rondino, A. Paladini, A. Giardini, A. Filippi and D. Catone, *Mass Spectrom. Rev.*, 2005, **24**, 588.
22 F. Lahmani, K. Le Barbu and A. Zehnacker-Rentien, *J. Phys. Chem. A*, 1999, **103**, 1991.
23 A. Latini, D. Toja, A. Giardini Guidoni, A. Palleschi, S. Piccirillo and M. Speranza, *Chirality*, 1999, **11**, 376.
24 A. A. Al-Rabaa, K. Le Barbu, F. Lahmani and A. Zehnacker-Rentien, *J. Phys. Chem. A*, 1997, **101**, 3273.
25 K. Le Barbu, V. Brenner, Ph. Millié, F. Lahmani and A. Zehnacker-Rentien, *J. Phys. Chem. A*, 1998, **102**, 128.
26 S. Piccirillo, M. Coreno, A. Giardini-Guidoni, G. Pizzella, M. Snels and R. Teghil, *J. Mol. Struct.*, 1993, **293**, 197.
27 T. M. Di Palma, A. Latini, M. Satta, M. Varvesi and A. Giardini Guidoni, *Chem. Phys. Lett.*, 1998, **284**, 184.
28 A. A. Al-Rabaa, E. Bréhèret, F. Lahmani and A. Zehnacker-Rentien, *Chem. Phys. Lett.*, 1995, **237**, 480.
29 F. Lahmani, K. Le Barbu-Debus, N. Seurre and A. Zehnacker-Rentien, *Chem. Phys. Lett.*, 2003, **357**, 636.
30 A. Latini, M. Satta, A. Giardini Guidoni, S. Piccirillo and M. Speranza, *Chem. Eur. J.*, 2000, **6**, 1042.

31 A. Giardini Guidoni, S. Piccirillo, D. Scuderi, M. Satta, T. M. Di Palma and M. Speranza, *Phys. Chem. Chem. Phys.*, 2000, **2**, 4139.
32 M. Mons, F. Piuzzi, I. Dimicoli, A. Zenhacker and F. Lahmani, *Phys. Chem. Chem. Phys.*, 2000, **2**, 5065.
33 N. Bohro, T. Haeber and M. A. Suhm, *Phys. Chem. Chem. Phys.*, 2001, **3**, 1945.
34 N. Bohro and M. A. Suhm, *Org. Biomol. Chem.*, 2003, **1**, 4351.
35 K. Le Barbu, F. Lahmani and A. Zehnacker-Rentien, *J. Phys. Chem.*, 2002, **106**, 6271.
36 N. Seurre, K. Le Barbu-Debus, F. Lahmani, A. Zehnacker-Rentien and J. Sepiol, *J. Mol. Struct.*, 2004, **692**, 127.
37 N. Seurre, J. Sepiol, K. Le Barbu-Debus, F. Lahmani and A. Zehnacker-Rentien, *Phys. Chem. Chem. Phys.*, 2004, **6**, 2867.
38 A. K. King and B. J. Howard, *Chem. Phys. Lett.*, 2001, **348**, 343.
39 D. Scuderi, A. Paladini, S. Piccirillo, M. Satta, D. Catone, A. Giardini, A. Filippi and M. Speranza, *Chem. Commun.*, 2002, 2438.
40 D. Scuderi, A. Paladini, S. Piccirillo, M. Satta, D. Catone, A. Giardini, A. Filippi and M. Speranza, *Phys. Chem. Chem. Phys.*, 2003, **5**, 4570.
41 D. Catone, A. Giardini Guidoni, A. Paladini, S. Piccirillo, F. Rondino, M. Satta, D. Scuderi and M. Speranza, *Angew. Chem., Int. Ed.*, 2004, **43**, 1868.
42 S. Piccirillo, M. Satta, D. Catone, D. Scuderi, A. Paladini, F. Rondino, M. Speranza and A. Giardini Guidoni, *Phys. Chem. Chem. Phys.*, 2004, **10**, 2858.
43 S. Piccirillo, F. Rondino, D. Catone, A. Giardini Guidoni, A. Paladini, M. Tacconi, M. Satta and M. Speranza, *J. Phys. Chem. A*, 2005, **109**, 1828.
44 D. Consalvo, A. Van der Avoird, S. Piccirillo, M. Coreno, A. Giardini Guidoni, A. Mele and M. Snels, *J. Chem. Phys.*, 1993, **99**, 8398.
45 M. J. Frisch, G. W. Trucks, H. B. Schlegel, G. E. Scuseria, M. A. Robb, J. R. Cheeseman, V. G. Zakrzewski, J. A. Montgomery, Jr., R. E. Stratmann, J. C. Burant, S. Dapprich, J. M. Millam, A. D. Daniels, K. N. Kudin, M. C. Strain, O. Farkas, J. Tomasi, V. Barone, M. Cossi, R. Cammi, B. Mennucci, C. Pomelli, C. Adamo, S. Clifford, J. Ochterski, G. A. Petersson, P. Y. Ayala, Q. Cui, K. Morokuma, D. K. Malick, A. D. Rabuck, K. Raghavachari, J. B. Foresman, J. Cioslowski, J. V. Ortiz, A. G. Baboul, B. B. Stefanov, G. Liu, A. Liashenko, P. Piskorz, I. Komaromi, R. Gomperts, R. L. Martin, D. J. Fox, T. Keith, M. A. Al-Laham, C. Y. Peng, A. Nanayakkara, C. Gonzalez, M. Challacombe, P. M. W. Gill, B. G. Johnson, W. Chen, M. W. Wong, J. L. Andres, M. Head-Gordon, E. S. Replogle and J. A. Pople, *GAUSSIAN 98 (Revision A.6)*, Gaussian, Inc., Pittsburgh, PA, 1998.
46 M. Shauer, K. S. Law and E. R. Bernstein, *J. Chem. Phys.*, 1985, **82**, 736.
47 M. Shauer, K. S. Law and E. R. Bernstein, *J. Chem. Phys.*, 1984, **81**, 49.
48 K. S. Law and E. R. Bernstein, *J. Chem. Phys.*, 1985, **82**, 2856.